

Lateral gating mechanism and plasticity of the β -barrel assembly machinery complex in micelles and *Escherichia coli*

Aathira Gopinath ^{a,b}, Tobias Rath^c, Nina Morgner ^c and Benesh Joseph ^{a,*}

^aDepartment of Physics, Freie Universität Berlin, Berlin, 14195, Germany

^bInstitute of Biophysics, Goethe Universität Frankfurt, Frankfurt, 60438, Germany

^cInstitute of Physical and Theoretical Chemistry, Goethe Universität Frankfurt, Frankfurt, 60438, Germany

*To whom correspondence should be addressed: Email: benesh.joseph@fu-berlin.de

Edited By: Ivet Bahar

Abstract

The β -barrel assembly machinery (BAM) mediates the folding and insertion of the majority of outer membrane proteins (OMPs) in gram-negative bacteria. BAM is a penta-heterooligomeric complex consisting of the central β -barrel BamA and four interacting lipoproteins BamB, C, D, and E. The conformational switching of BamA between inward-open (IO) and lateral-open (LO) conformations is required for substrate recognition and folding. However, the mechanism for the lateral gating or how the structural details observed in vitro correspond with the cellular environment remains elusive. In this study, we addressed these questions by characterizing the conformational heterogeneity of BamAB, BamACDE, and BamABCDE complexes in detergent micelles and/or *Escherichia coli* using pulsed dipolar electron spin resonance spectroscopy (PDS). We show that the binding of BamB does not induce any visible changes in BamA, and the BamAB complex exists in the IO conformation. The BamCDE complex induces an IO to LO transition through a coordinated movement along the BamA barrel. However, the extracellular loop 6 (L6) is unaffected by the presence of lipoproteins and exhibits large segmental dynamics extending to the exit pore. PDS experiments with the BamABCDE complex in intact *E. coli* confirmed the dynamic behavior of both the lateral gate and the L6 in the native environment. Our results demonstrate that the BamCDE complex plays a key role in the function by regulating lateral gating in BamA.

Keywords: BAM complex, protein folding, spin labeling, conformational dynamics, in-cell EPR

Significance Statement

The β -barrel assembly machinery (BAM) complex, which consists of the central β -barrel BamA and four other lipoproteins (BamB–E), performs protein folding and insertion into the bacterial outer membrane. BAM is a potential target for new antibiotics. The gating of BamA between an inward-open (IO) and a lateral-open (LO) conformation is essential for function. The conformational plasticity of BamA lead to the appearance of various conformations in the structures and differing views on the gating mechanism. We show that BamAB adopts an IO conformation, whereas the binding of BamCDE subcomplex induces the lateral opening in BamA. Using in situ spectroscopic measurements, we show that these dynamic changes are conserved in intact *Escherichia coli* cells.

Introduction

Gram-negative ESKAPE pathogens, which are a group of antibiotic-resistant pathogens, constitute a major threat to human health worldwide (1). They have a unique outer membrane (OM) as a selective barrier to protect against harmful external factors including antibiotics. The OM is an asymmetric bilayer consisting of phospholipids and lipopolysaccharides. In addition, it carries numerous β -barrel proteins (known as OM proteins or OMPs) performing crucial biological functions. OMPs are also present in mitochondria and chloroplasts and altogether they perform a wide range of functions including transport of nutrients, signaling, motility, membrane biogenesis, protein import, and

secretion among others (2, 3). The proper assembly and maintenance of OMPs are crucial for bacterial survival and virulence. The folding and insertion of the majority of the OMPs are mediated by the β -barrel assembly machinery (BAM) (4–10). BAM is a penta-heterooligomeric complex composed of five components, namely BamA, BamB, BamC, BamD, and BamE (11–14). BamA, which is a 16-stranded β -barrel forms the central component (11, 15–17). The four other lipoproteins (BamB–E) interact with the polypeptide transport-associated domains (POTRA 1–5 named as P1–P5) of the BamA at the periplasmic side (18–20). The unfolded OMPs (uOMPs) in complex with the chaperone interact with BAM in the periplasm (21, 22), and subsequently, the uOMP is folded

Competing Interest: The authors declare no competing interest.

Received: October 9, 2023. **Accepted:** January 8, 2024

© The Author(s) 2024. Published by Oxford University Press on behalf of National Academy of Sciences. This is an Open Access article distributed under the terms of the Creative Commons Attribution License (<https://creativecommons.org/licenses/by/4.0/>), which permits unrestricted reuse, distribution, and reproduction in any medium, provided the original work is properly cited.

and inserted into the OM (10, 23–25). BamA and BamD are conserved (4), whereas the precise function of the other lipoproteins remains elusive. Due to the presence of BAM complex in all gram-negative bacteria including the ESKAPE pathogens, it is a potential target for novel antibiotics (26–30).

The crystal structure of the BamACDE complex revealed BamA in the lateral-open (LO) conformation, and it was suggested that BamCDE binding induces the opening of the lateral gate and exit pore in BamA (18). A subsequent structure further confirmed the LO conformation of the BamACDE complex (19). In both of these works, BamB was lost during incubation for crystallization. However, in the above work, the BamABCDE full complex was observed in the inward-open (IO) conformation and it was suggested that BamB, but not BamCDE may regulate the lateral gating of BamA. Adding further to this ambiguity, a subsequent cryo-electron microscopy (cryo-EM) structure revealed the BamABCDE full complex in the LO conformation (31). Though the cycling between IO and LO conformations is essential for BAM function (25, 31–33), how this is achieved and regulated remains elusive.

The observations above altogether show that the BamA barrel is a very dynamic structure and adopts a specific conformation in response to changes in its subunit composition and/or the surroundings. Structures captured distinct states from this broad conformational space. Interestingly, when observed in the native OMs, BamA showed a heterogeneous conformation spanning multiple states (34). A systematic observation of BamAB, BamACDE, and BamABCDE complexes under identical conditions is necessary to exclude the differential effects of the environments and to elucidate the gating mechanism. The in vitro observations also need to be validated in the cellular environment when feasible. In this study, we achieved these goals by observing BamAB, BamACDE, and BamABCDE complexes in detergent micelles using pulsed electron–electron double resonance (PELDOR or DEER) spectroscopy. Further, the conformation and heterogeneity of the key structural elements in BamA were examined by observing the BamABCDE complex in intact *Escherichia coli* using in situ PELDOR spectroscopy (35–37). Our results provide detailed structural and dynamic information for these complexes and show that BamCDE, but not BamB binding switches BamA into the LO conformation both in vitro and in situ.

Results

Observing the conformation of BAM sub/full complexes using DEER/PELDOR spectroscopy

The BamAB, BamACDE, and BamABCDE complexes eluted as a monodisperse peak from the size-exclusion chromatography (SEC) column. The individual subunits were well resolved for all of them as observed from sodium dodecyl-sulfate polyacrylamide gel electrophoresis (SDS-PAGE) (Fig. S1A and B). We further identified these complexes using laser-induced liquid bead ion desorption mass spectrometry (LILBID–MS) (38, 39). The native-MS data also revealed that BamA can form stable interactions with one to four lipoproteins in various combinations (Fig. S1C). Electron spin resonance (ESR or EPR) spectroscopy techniques constitute a versatile set of tools to study biomolecules, in particular for membrane proteins under both in vitro and in situ conditions (40–44). Conventionally, nitroxide-based spin labels are engineered at desired sites through the reaction of a thiosulfate-functionalized spin label with a cysteine residue. Here we used the methanethiosulfonate spin label (MTSL) to selectively label BamA at positions located on the extracellular-, β -barrel-, and the periplasmic regions (Figs. 2–6, panels A). The distance

distribution between such engineered spin pairs was determined using DEER/PELDOR spectroscopy (45, 46). We chose several positions based on the available structures such that the different conformations of BamA can be selectively observed for BamAB, BamACDE, and BamABCDE complexes. A Cys-less variant of BamA was created for this purpose after substituting the two native cysteines (at positions 690 and 700) for a serine, which was shown to least affect the function (31). At the extracellular side, the β 16 strand (at position Q801C) was paired with loop 1 (L1, at position T434C). L1 was also connected with L6 (at position S690C) and L8 (at position G796C). The L8 was connected with L3 (at position L501C) as well. At the periplasmic side, turn 1 (T1, at position T452C) was coupled to turn 6 (T6, at position S732C). To monitor the orientation of the POTRA 5, position T359C was paired with turn 7 (T7, at position L780C). To further characterize the BamABCDE complex, additional spin pairs were engineered. The L1 was connected to L6 through the T434C–S657C and T434C–S700C pairs. The internal dynamics of L6 were further probed using the S690C–S700C variant. The L3 (L501C) was connected to L6 (at position S700C), L7 (at position S751C), and β 16 (at position Q801C). All these variants were purified into n-dodecyl β -maltoside (DDM) micelles and could be labeled using MTSL with high efficiency (Table S1). For observing the BamABCDE complex in *E. coli*, L1–L8 (T434C–G796C), L3–L6 (L501C–S690C, L501C–Q693C), L3–L7 (L501C–S751C), L3–L8 (L501C–G769C), and L4–L8 (D562C–G796C) variants were used. Simulations (see Materials and methods) on the structures (PDBs 5D00, 5LJO, and 6V05) revealed very high accessibility (hence the least perturbation, if any) as well as distinct distances corresponding to the IO and LO conformations for all the pairs. The Cys-less and/or single cysteine variants were used as the control samples. All the variants supported the growth of *E. coli* cells having the native BamA expression controlled with an arabinose promoter (Fig. S2).

BamA exhibits distinct response to lipoproteins at different positions along the barrel

The overall dynamics (in the ps–ns timescale, including the motion of the label itself, side chain, backbone, and the protein) at the spin-labeled site are encoded into the room temperature continuous wave (RT CW) ESR spectrum. As the overall motion gets faster, the spectrum is narrower, and vice versa. Thus, such spectra can provide information on site-specific variation of dynamics or its modulation by other interacting partners at physiological temperatures (47). We obtained RT CW ESR data using doubly labeled variants of BamAB, BamACDE, and BamABCDE at a few key positions (Figs. 1 and S3). As the spectra are a superposition of signals from the two labeled sites, it gives an averaged value for the overall change in dynamics. Nevertheless, it allows for a direct comparison with the conformational changes observed from the DEER/PELDOR data (presented in the latter sections). For the lateral gate (434–801), a comparative observation of the data shows spectral narrowing for BamACDE and BamABCDE (Fig. 1). This reveals increased dynamics as compared to BamAB, which is in line with an opening of the lateral gate in both BamACDE and BamABCDE (19, 31). For a more quantitative analysis, we extracted the corresponding correlation times (τ_c) through a multi-parameter fitting (overlaid in red dotted lines) of the spectra (48). These τ_c values provide a useful parameter to compare the overall dynamics between different states observed. At the lateral gate, this gave a τ_c of 4.5 ± 0.9 ns in BamAB, which decreased to 3.5 ± 0.7 ns for the other two complexes (Table 1).

For the P5–T7 pair (359–780) we see an opposite response where the dynamics are reduced (with increased spectral width) in the BamACDE and BamABCDE complexes ($\tau_c = 5.6 \pm 1.2$ ns) in relation to BamAB ($\tau_c = 4.5 \pm 0.9$ ns). This agrees with the P5 closed conformation for BamACDE and BamABCDE as observed in the LO structures and the dynamic changes previously observed from a

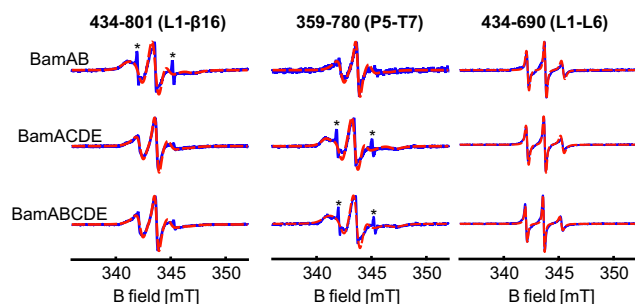


Fig. 1. RT CW ESR spectra of the selected positions for BamAB, BamACDE, and BamABCDE in DDM micelles. Simulations obtained using the EasySpin program are overlaid (in dotted lines) and the corresponding correlation time values are given in Table 1. The asterisks indicate a signal from a small fraction of free spin labels.

Table 1. Correlation times were obtained for the selected spin-labeled BAM subcomplex and full complex variants using RT CW ESR spectroscopy.

BAM sub/full complex	Spin labeled variants		
	434-801 (L1-β16)	359-780 (P5-T7)	434-690 (L1-L6)
Correlation time (τ_c), ns			
AB	4.5 ± 0.9	4.5 ± 0.9	0.9 ± 0.2
ACDE	3.5 ± 0.7	5.6 ± 1.2	1.0 ± 0.2
ABCDE	3.5 ± 0.7	5.6 ± 1.2	1.0 ± 0.2

The corresponding spectra and simulations are shown in Fig. 2.

solid-state NMR study (19, 31, 49). Strikingly, the L1–L6 pair (434–690) gave a very narrow spectrum revealing significantly enhanced dynamics. Position 434 was also used to observe the lateral gate (434–801), but did not produce such a narrow component. Therefore, narrowing must be contributed by the MTSL attached to position 690, and with its extremely narrow feature it dominated the overall shape of the spectrum. Simulations gave the smallest correlation time among all the samples investigated (1.0 ± 0.2 ns). Position 690 is located (in a nonconserved insertion) on L6, which is essential for function (15, 50). A previous NMR study showed enhanced backbone dynamics at this insertion sequence (51) and our observations reveal such a behavior for the side chain as well. Overall, the dynamics and its modulation by the lipoproteins at the lateral gate and P5 suggest an IO (in BamAB) to LO (in both BamACDE and BamABCDE) transition, which very well corresponds with the conformational changes and heterogeneity characterized using PELDOR spectroscopy (Figs. 2–6).

The lateral gate is closed in BamAB and remains open in BamACDE and BamABCDE

To probe the effect of lipoproteins for the gating of the BamA lateral gate, we used the 434–801 and 434–796 variants (Figs. 2A, S4, and S5). Position 801 is located at the β16 and 796 is located five amino acids away on L8. These pairs show a large change in the interspin distances between the IO and LO conformations. For 434–801 in BamAB, the PELDOR data revealed a short interspin distance (r_{\max} at 1.5 nm), which is in good agreement with simulations for the IO conformation (Fig. 2B). For BamACDE and BamABCDE, the distance significantly increased (r_{\max} at 3.0 and 3.1 nm, respectively) in agreement with simulation for the LO conformation as well as the increased dynamics observed from the CW ESR spectra (Fig. 1). Similar results were observed for the 434–796 pair (Fig. 2C). In BamAB, it gave distances close to the simulation for the IO conformation (r_{\max} at 2.2 nm) and in

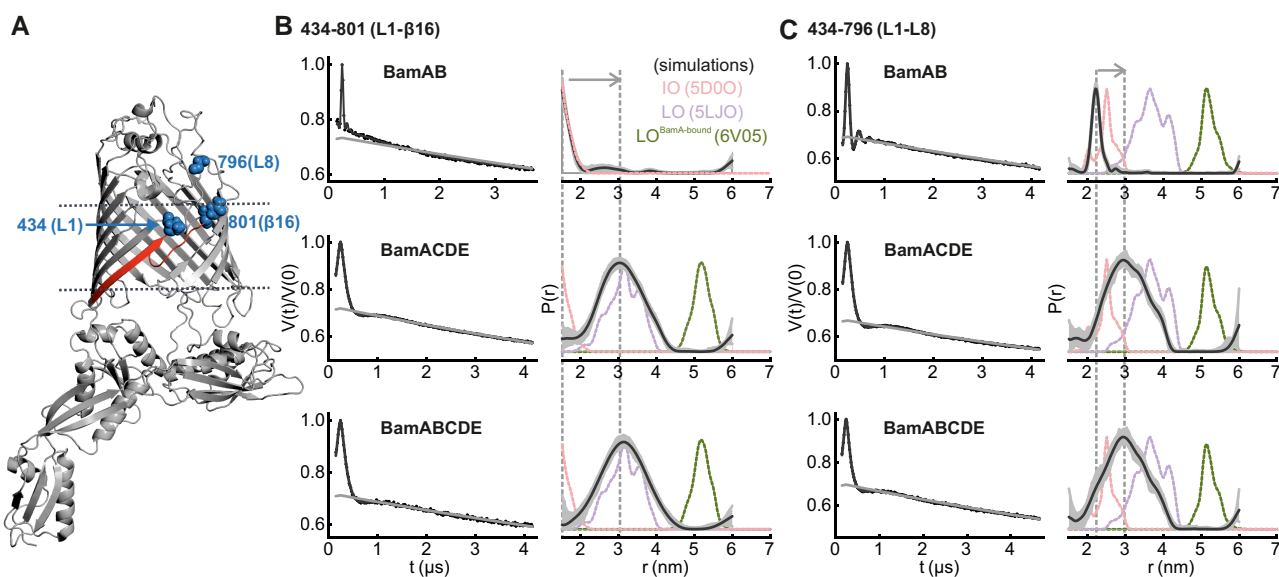


Fig. 2. DEER/PELDOR data for the lateral gate in BamAB, BamACDE, and BamABCDE in DDM micelles. A) Structure of BamA in an IO conformation (PDB 5D00). The lateral gate region (red) and the spin-labeled positions (blue spheres) are highlighted on the structure. The lipoproteins are not shown for clarity. B and C) Primary data overlaid with the fits obtained using the DeerLab (52) program are shown in the left panels. The obtained distance distributions with a 95% confidence interval are shown on the right. Simulations for the IO (PDB 5D00), LO (PDB 5LJO), and $\text{LO}^{\text{BamA-bound}}$ conformations (PDB 6V05) are overlaid in dotted lines.

BamACDE and BamABCDE, the mean distance increased with a broad distribution (r_{\max} at 2.9 nm) similar to the LO conformation.

L3, L7, and L8 are less flexible and L6 occupies a broad conformational space in detergent micelles

In the available structures, the L3 is seen to undergo large conformational changes between different conformations of BamA barrel. In the structures, the L3–L8 distances increased by >1 nm upon changing from the IO to the LO conformation (501–796, Fig. S5A and B). However, in one of the substrate-bound conformations (LO^{BamA-bound}, in which the lateral gate further opened, Figs. 3A and S5C), the L3 moved back into the barrel (23). In BamAB, the L3–L8 (501–796) PELDOR data gave a narrow distribution (r_{\max} at 1.9 nm), shorter than the range predicted for the IO conformation (Fig. 3B). The narrow width of the distribution reveals a rigid orientation of both L3 and L8. Strikingly, for both BamACDE and BamABCDE in which the lateral gate is open (Fig. 2B and C), the distances further decreased (r_{\max} at 1.5 nm), revealing a tightly closed conformation of L3 over the barrel lumen (similar to that observed in the LO^{BamA-bound} conformation). This is in stark contrast to the expected opening of L3 as observed in the LO structures (10, 19, 24, 25, 53). To further verify this observation, we used the L3– β 16 (501–801), L3–L6 (501–700), and L3–L7 (501–751) pairs and determined the distances in the BamABCDE complex. For L3–L7, overall, the observed distance distribution is shorter (r_{\max} at 2.5 nm) than the simulation for the IO (and LO) conformation (Fig. 3C). The narrow distribution of L3–L7 distances reveals a rather rigid orientation of L7 as well. For L3– β 16, the distances lie closer to the IO (and LO^{BamA-bound}) conformation (r_{\max} at 3.0 nm, Fig. 3D). Thus, we did not observe the open conformation of L3 in all three variants above. Notably, the L3–L6 pair revealed a very broad distribution covering different conformations as observed in the available structures (Fig. 3E). The longer distances overlap with simulations for the IO and LO conformations,

whereas a major part of the distribution is much shorter (as in the LO^{BamA-bound} structure), revealing an orientation of L3 very close to L6 over the barrel lumen. Considering the rigid orientation of L3, the broadness must be accounted by the dynamics of L6, which is also suggested from the CW ESR spectra (Fig. 1 and also see Fig. 4). Combined with the results for the lateral gate (which evidently switches between IO and LO conformations, Fig. 2), these observations reveal that BamA is a very dynamic structure and its key functional elements exhibit distinct changes in response to the presence of lipoproteins and/or the nature of the surrounding environment.

L6 is insensitive to the lipoproteins and spans a broad conformational space

In view of the broad L3–L6 distribution as observed above, we further investigated the conformational heterogeneity of L6 by engineering more inter- and intraloop spin pairs (Fig. 4A). The L6 forms the longest extracellular loop in BamA of *E. coli*. It covers the barrel from the extracellular side and is essential for the function of the BAM complex (11). L6 contains two cysteines at positions 690 and 700, which can naturally form a disulfide bond. These cysteines were substituted in several studies, which did not affect the function (11, 31, 32). First, we investigated the effect of lipoproteins on the L6 conformation using the L1–L6 (434–690) variant. In BamAB, it gave a very broad distribution (r_{\max} at 3.8 nm) spanning distances much longer than the IO and LO conformations. The lower part of the distribution corresponds to an overlay of the distances for the IO, LO, and EspP-bound (LO^{EspP-bound}) conformations (24), and the remaining part reveals a continuum of conformations having L6 placed further away from L1 (Fig. 4B). Very interestingly, this distribution showed little changes when observed in BamACDE or BamABCDE, revealing that the L6 conformation is insensitive to the binding of lipoproteins. Though position 434 (L1) shows a large outward

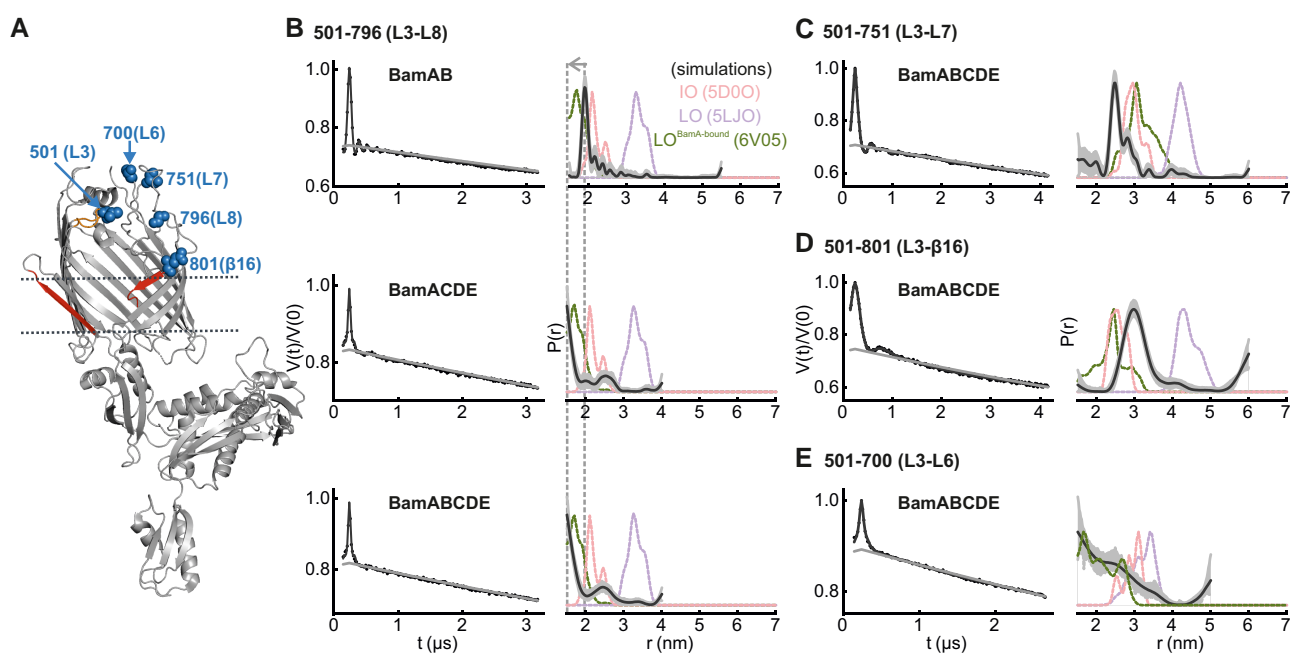


Fig. 3. DEER/PELDOR data for the extracellular loop 3 (L3) in BamAB, BamACDE, and/or BamABCDE in DDM micelles. A) Structure of BamA in the LO^{BamA-bound} conformation (PDB 6V05). The lateral gate region (in red) is open to the membrane with L3 (in orange) inside the lumen. The spin-labeled positions (blue) are highlighted as spheres. The lipoproteins and the substrate are not shown for clarity. B–E) Primary data overlaid with the fits obtained using the DeerLab (52) program are shown in the left panels. The obtained distance distributions with a 95% confidence interval are shown on the right. Simulations for the IO (PDB 5D00), LO (PDB 5LJO), and LO^{BamA-bound} conformations (PDB 6V05) are overlaid in dotted lines.

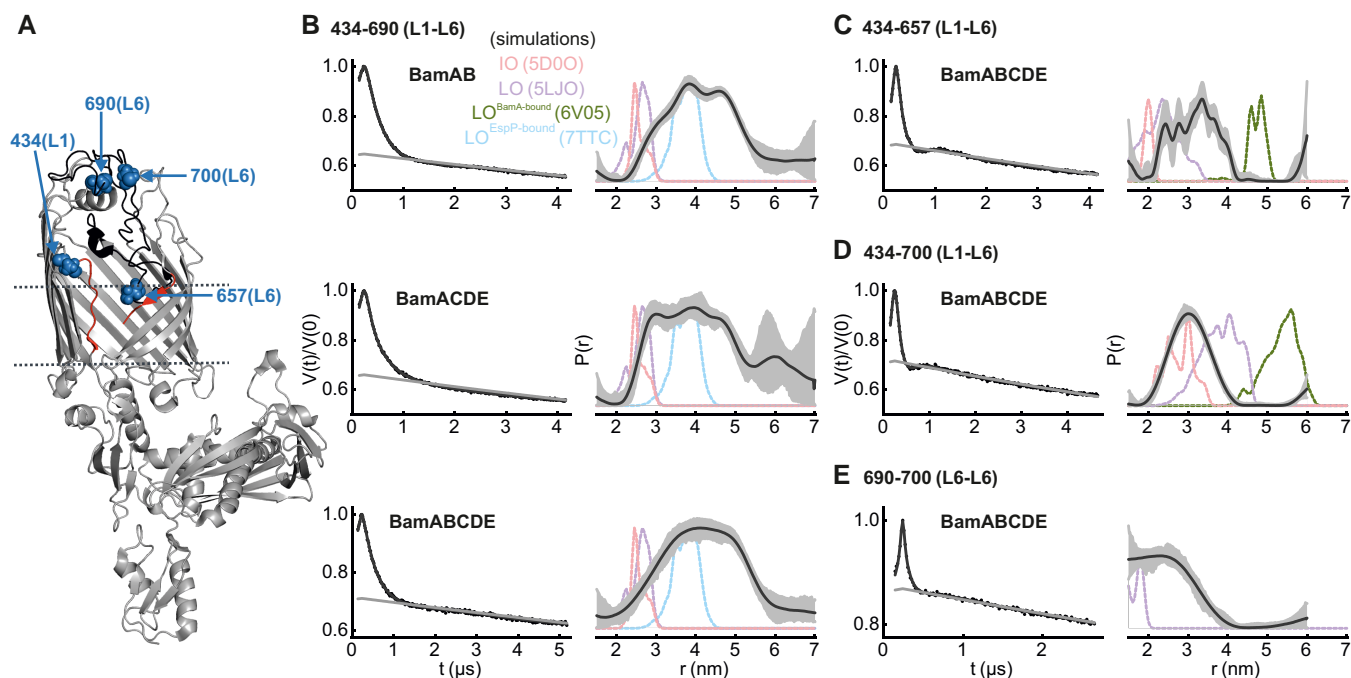


Fig. 4. DEER/PELDOR data for the extracellular loop 6 (L6) of BamAB, BamACDE, and BamABCDE in DDM micelles. A) Structure of BamA in the LO conformation (PDB 5LJO). The lateral gate region (red) is open to the membrane and L6 (black) spanning the extracellular side. The spin-labeled positions (blue) are highlighted as spheres. The lipoproteins are not shown for clarity. B–E) Primary data overlaid with the fits obtained using the DeerLab (52) program are shown in the left panels. The obtained distance distributions with a 95% confidence interval are shown on the right. Simulations for the IO (PDB 5D00), LO (PDB 5LJO), $\text{LO}^{\text{BamA-bound}}$ (PDB 6V05), and $\text{LO}^{\text{EspP-bound}}$ (PDB 7TTC) conformations (as available) are overlaid in dotted lines.

displacement during the IO to LO transition, distances to position 690 (L6) do not appreciably change due to a similar relative orientation (see the corresponding simulations in Fig. 4B). Also, 434 (L1) distances to other positions show good agreement with the simulations (Fig. 2B and C). Thus, the broadening of L1–L6 distribution must be mostly contributed through the dynamics of L6.

In *E. coli*, residues 685–697 correspond to a nonconserved insertion into the L6 (51), which is located at the top of the barrel into the extracellular space. We designed two variants in which L6 is labeled away from the lower and upper ends of the insertion (Fig. 4C and D). One of these variants (434–657) also gave a distribution significantly broader than the IO and LO simulations. Position 657 is located in a region inside the barrel close to the lateral gate and forms an exit pore together with L1–L3 for the release of extracellular regions of the folding substrate. Thus, the segmental dynamics of L6 are transduced beyond the insertion sequence toward the key functional regions inside BamA. The other variants (434–700) gave distances that are comparatively less broad, revealing reduced dynamics at position 700 (as compared to position 690). We further probed the internal dynamics of this region using wild-type (WT) BamABCDE having the native cysteines retained. A significant fraction (~40%) of the molecules could be spin-labeled at these positions following incubation with β -mercaptoethanol. It showed a rather broad distance distribution (Fig. 4E) and the disulfide bond might restrict this interresidue (690–700) dynamics in the WT protein. Therefore, the removal of the native disulfide bond in L6 might account for the enhanced dynamics we observed. When the cysteines were substituted, this region had a poor resolution in BamA/BAM structures (15, 16, 23, 53, 54), revealing increased flexibility as we observed. Overall, our observations show that the native disulfide bond has an important role in the regulation of dynamics in L6. Though it would be informative to perform the other distance measurements with

this disulfide bond retained (to directly dissect the role of the disulfide bond for L6), possible nonspecific labeling of the native cysteines precluded such experiments.

BamCDE, but not BamB binding closes periplasmic turns and POTRA 5 in BamA

We probed the response of the periplasmic turns T1 and T6 to the binding of lipoproteins using the 452–732 variant (Figs. 5A and S5). In BamAB, the interspin distances (r_{max} at 3.9 nm) are similar to the simulation for the IO structure. However, in BamACDE and BamABCDE, the distances decreased (r_{max} at 3.3 nm) revealing the closure of these turns in line with the simulation for the LO conformation (Fig. 5B). Overall, the distribution is broader than the simulation, which reveals increased flexibility of these turns in the LO conformation. We further probed the response of POTRA 5 using the 359–780 (P5–T7) variant. Again, in BamAB, the experimental distribution (r_{max} at 3.6 nm) is overlaid with the IO simulation. However, in BamACDE and BamABCDE, the distances were significantly decreased (r_{max} at 1.5 nm), revealing the movement of POTRA 5 toward the barrel lumen as observed in the LO conformation (Figs. 5B and S4). This is also in line with the reduced mobility at these positions for BamACDE and BamABCDE complexes as observed from the CW ESR spectra (Fig. 1). Altogether, our observations confirm that BamCDE, but not BamB shifts BamA barrel into the LO conformation.

Conformation of L3, L6, and the lateral gate in *E. coli*

Earlier we demonstrated that for OMPs, the structural and conformational changes can be observed in intact *E. coli* and isolated OMs using in situ spin labeling and PELDOR experiments (37, 55, 56). Solid-state NMR and single-molecule force spectroscopy

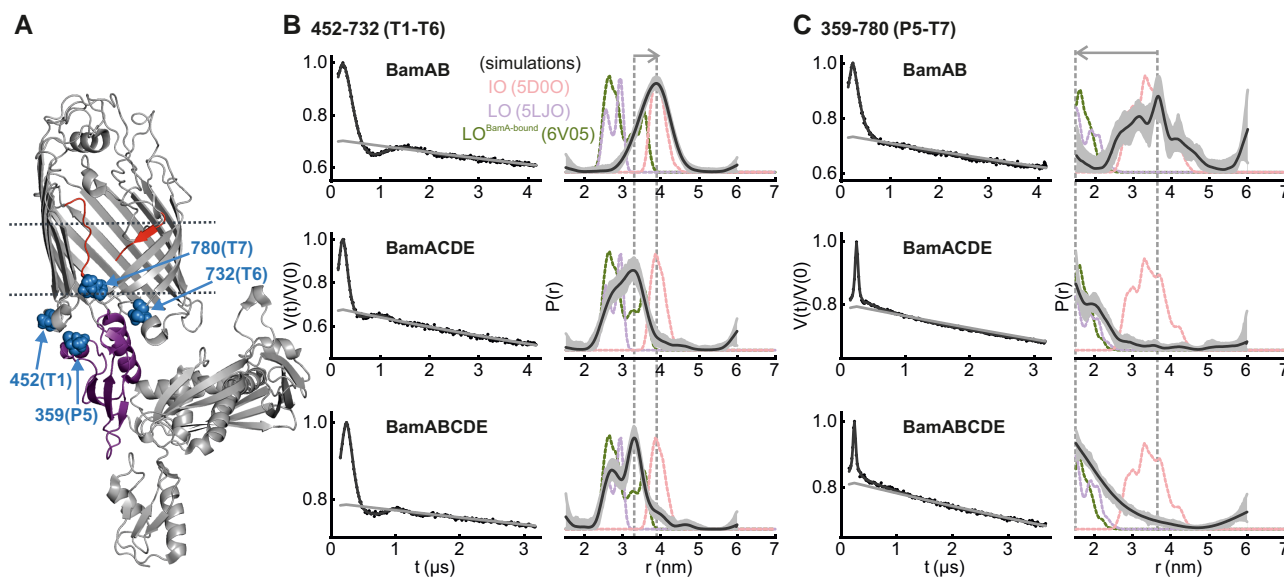


Fig. 5. DEER/PELDOR data for the periplasmic gate (T1–T6) and between P5–T7 of BamAB, BamACDE, and BamABCDE in DDM micelles. A) Structure of BamA in the LO conformation (PDB 5LJO). The POTRA5 (in purple) and the spin-labeled positions (in blue spheres) are highlighted. B and C) Primary data overlaid with the fits obtained using the DeerLab (52) program are shown in the left panels. The obtained distance distributions with a 95% confidence interval are shown on the right. Simulations for the IO (PDB 5D00), LO (PDB 5LJO), and LO^{BamA-bound} conformations (PDB 6V05) are overlaid in dotted lines.

techniques are complementary tools for such investigations, in particular for isolated OMs (57, 58). Using this approach, we showed that BamA displays an increased heterogeneity, in particular at the lateral gate when observed in the native outer membranes (34). Here, we extended similar experiments for many other interloop pairs of BamABCDE full complex in intact *E. coli* cells (Figs. 6 and S6–S10). Spin labeling is rather limited to the surface-exposed cysteines in *E. coli*. The L3 was connected to L6 using the 501–690 and the 501–693 variants. Both of them gave a probability distribution significantly broader (r_{\max} at 3.0 and 2.8 nm, respectively) than the simulations for the IO and LO conformations (Fig. 6B and C). Thus, the segmental dynamics of L6 observed in DDM micelles (Fig. 4) are preserved in the cellular environment. For the L3–L7 pair (501–751), the experimental distribution lies closer to the simulation for the IO (or LO^{BamA-bound}) conformation, but is significantly broader than both the simulation and the detergent solubilized sample (Fig. 6D). In agreement, the L3–L8 (501–796) distribution is also appreciably longer and broader than the results in detergent micelles and the IO simulation (Fig. 6E). The overall distribution is more centered at the IO conformation and a small fraction of distances overlaps with the simulation for the LO conformation. For L4–L8 (562–796), simulations cannot differentiate between IO and LO conformations, and the experimental distribution overlaps with both simulations (revealing an overall limited flexibility for both L4 and L8).

The above observation implies that the increased width for the L3–L8 (501–796, and possibly for L3–L7/501–751) distribution is attributed to an enhanced flexibility of L3. Importantly, the L1–L8 pair (434–796) reporting at the lateral gate revealed a broad distribution in *E. coli* covering the range corresponding to both IO and LO conformations, suggesting equilibrium between closed and open conformations (Fig. 6G). Overall, the distances are significantly broader and longer than the corresponding distribution for BamAB observed in DDM micelles (Fig. 2C and overlaid in Fig. 6G). We could not verify the subunit composition of BAM for the experiments in *E. coli*. An identical expression protocol was used for the *in vitro* purification, which gave the intact BAM

complex (Fig. S1A–C). Thus, BamA might interact with all of the Bam lipoproteins to form the full complex under the expression conditions. Under a laboratory environment, BamA and the lipoproteins are expressed at a few thousand ($1.5\text{--}6.0 \times 10^3$) copies per cell (61). In our case, overexpression leads to a 100-fold increase in the copy number for BamA (34), which is comparable to the native expression level of some of the OMPs (such as OmpA, OmpC, and OmpF). As for membrane protein overexpression in general, the cells may increase the surface area to accommodate the additional copies of BAM molecules (62). Importantly, our control experiments using single cysteine variants did not give any particular distances (Fig. S6), revealing a sufficient separation between individual BAM molecules in the native OM.

Discussion

Despite the large amount of structural data available, the exact role of the lipoproteins in the structure and dynamics of BamA remains elusive. While structures for BamA, BamACDE, and BamABCDE complexes are available, BamAB or other possible subcomplex structures with BamA have not yet been observed. The heterogeneity of BamA conformation observed in various structures leads to differing ideas regarding the role of lipoproteins in BamA gating. Here, we specifically addressed the role of lipoproteins on the dynamics and structure of BamA and further corroborated those observations with results obtained in intact *E. coli*.

While structures provide distinct snapshots from the conformational space, the associated changes in dynamics are obscured. The RT CW ESR spectroscopy data showed that in comparison to BamAB, the overall dynamics are increased at the lateral gate (L1– β 16/434–801, Fig. 1) for BamACDE and BamABCDE. This is accompanied with decreased dynamics for the P5–T7 pair (359–780). These observations agree with the IO to LO transition at the lateral gate induced by BamCDE binding. Here, the P5 moves into a closed conformation toward the barrel, and the β 1– β 6 strands rotate outward into the LO conformation. These changes are in perfect

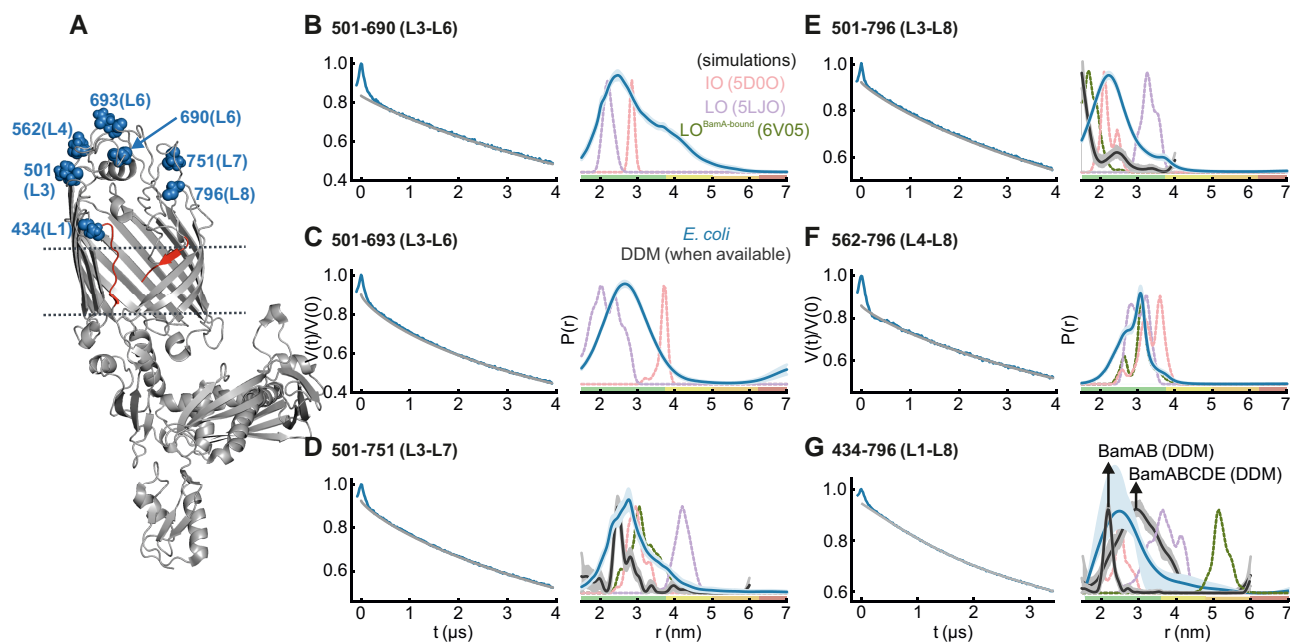


Fig. 6. DEER/PELDOR data for the lateral gate and between the extracellular loops of BamABCDE complex in intact *E. coli*. A) Structure of BamA in the LO conformation (PDB 5LJO) as explained in Fig. 4A. B–F) Primary data overlaid with the background function (in gray) obtained using the DEERNet (59) program are shown in the left panels. Analysis employing TR also gave a similar distance distribution (Fig. S8). G) For the lateral gate (434–796), a polynomial background correction as determined from the corresponding single cysteine variants was employed for TR using the DeerAnalysis program (60) (see Fig. S7B). The DEERNet also predicted a similar distribution except for an additional small peak at longer distances, which was disregarded in view of the limited observation window of the dipolar evolution. The obtained distance distributions with an uncertainty band are shown on the right. The color code relates the reliability of different features of the probability distribution with the length of the observed dipolar evolution time. In the green zone, shape, width, and the mean distance are accurate. In the yellow zone, the width and the mean, and the orange zone, the mean distance is reliable. Distances distribution in DDM (when available) and simulations for the IO (salmon, PDB 5D00), LO (light violet, PDB 5LJO), and LO^{BamA-bound} (green, PDB 6V05) conformations are overlaid in dotted lines. The corresponding control measurements employing single cysteine variants are shown in Fig. S7. Another fully independent set of replicates produced similar results (Figs. S9 and S10).

agreement with the DEER/PELDOR results. BamCDE binding induced an opening of the lateral gate with a concomitant closure of P5 (plus T1 and T6, Figs. 2 and 5) into the barrel lumen. BamB binding alone did not induce any visible changes in BamA. Thus, BamB might have an accessory role in facilitating substrate recognition, folding, or interaction with the SurA chaperone in the periplasm (21).

Although the lateral gate of BamA opens upon BamCDE binding, the L3 showed an independent response. In BamAB, it gave a narrow distance distribution against L8, which is closer than the conformation observed in the IO structure. BamCDE binding further decreased the distance, revealing an even more closed conformation of L3 over the barrel and nearer to L8 as observed in the LO^{BamA-bound} structure (Fig. 3). Thus, the opening of the lateral gate (Fig. 2, as well as the closure of P5, T1–T6, Fig. 5) and the outward motion of L3 following BamCDE binding (as observed in the structures) might not be strictly correlated events. The L3 might be sensitive to the surrounding environment and the presence of the substrate, which also might explain its varying conformations between different structures. Notably, when BamA was expressed without any lipoproteins, L3 displayed a dynamic behavior spanning the range of both IO and LO conformations in the native outer membranes (34). A rather narrow interloop distance distribution against the rigid L3 reveals limited flexibility for L7 and L8 as well (Fig. 3B and C). Such a stable orientation of L3, L7, and L8 might restrict nonspecific diffusion of molecules through the barrel lumen. On the other side, the very broad distance distribution for positions on L6 revealed an extremely dynamic behavior starting at the nonconserved insertion sequence (residues 685–697) and extending toward the exit pore close to

the lateral gate (Fig. 4), also in a manner fully independent to the presence of the lipoproteins (Fig. 4B, see Discussion).

In *E. coli*, the L3 has a more flexible behavior, distinct from its rather rigid conformation in micelles and several structural snapshots (Fig. 6B–E). Yet, it remains nearer to the closed conformation over the barrel lumen. The enhanced segmental flexibility of L6 is preserved in *E. coli*, validating its relevance in the physiological surroundings. A previous molecular dynamics study suggested a fixed orientation of L6 in BamA (32). We did not observe BamA alone and also removed the native disulfide bond (between residues 690 and 700), which would increase the overall flexibility (Fig. 4E). Also, this region had poor resolution in the structures when the native cysteines were substituted (15, 16, 23, 53, 54). Thus, the native disulfide bond has a key role in regulating the overall dynamics of L6. This bond is intact in most of the available structures; however, the cysteines remained nonbonded in some of them (19, 31, 63). Thus, the cysteines may also switch between bonded and nonbonded states depending on the redox state of the surrounding vicinity and thereby modulate the segmental dynamics in L6. Together with L1 and L2, L3 and L6 form a putative substrate exit pore over the BamA barrel (32). In the closed conformation, they might prevent nonspecific diffusion of molecules through the barrel lumen. However, these loops move out to accommodate and release the structural elements of the substrate during protein folding (32, 64). The flexible nature of these loops might ensure that they can regulate the accessibility of the barrel lumen in a substrate-dependent manner. The well-conserved VRGF motif (residues 660–663) in L6 is located at the exit pore interface, and our data (at the nearby position 657) suggest that the absence of the disulfide bond increases the flexibility of this

region (Fig. 4C). This may have a direct effect on the binding and/or release of substrate(s) at the lateral gate. Whether a redox transition of the native disulfide bond and the associated conformational changes have a role in function or combating challenges in the environment (such as the envelope stress due to external factors) (64) requires further investigations.

In *E. coli*, the lateral gate of BamA showed a heterogeneous conformation including both open and closed conformations (Fig. 6G, 434–796). At the moment, it is unclear to us whether the lipoprotein(s) binding can shift the conformational equilibrium at the lateral gate of BamA in *E. coli*. The data suggest a somewhat smaller opening as compared to the micelles. A stable opening of the lateral gate within the membrane plane might be favored through an interaction with the folding strand(s) of the substrate. This would in turn induce conformational changes at the exit pore including that of L3 (which is closed otherwise) and L6 allowing the release of the extracellular regions of the folded substrate. Although the in situ data qualitatively validated the conformation of L3, L6, and the lateral gate observed in micelles, several positions showed significant differences in the overall structural heterogeneity (in comparison to micelles and/or the structures, Fig. 6). In *E. coli*, interaction with the lipopolysaccharide, asymmetric OM, and/or the native substrate(s) may affect the observed conformation. When observed in the native-like membranes using molecular dynamics simulations, BamA displayed occasional spontaneous opening of the lateral gate (33, 65). Also, BAM and the surrounding lipids mutually interact leading to the modulation of their dynamics and the function of BAM (11, 33, 66–69). Thus, it would be informative to perform similar experiments in different lipid bilayers including the native outer membranes, which is beyond the scope of the current investigation.

In summary, BamA and BamAB adopt an IO conformation, and binding of BamCDE is correlated with the closure of P5, T1, and T6 into the barrel lumen and opening of the lateral gate in BamA (Fig. 7). In the native environment BamCDE binding might enhance lateral opening and subsequent protein insertion (33, 34, 65). Importantly, for both BamACDE and BamABCDE complexes, the barrel adopts the LO conformation. In view of the available structural and biophysical data as well as the results presented here, the IO conformation of the BamABCDE complex (19) might

have been favored by the crystallization conditions. BamD interacts directly with P5 and thereby might drive opening of the lateral gate, which is necessary for function (25, 31, 32). Thus, our observations also provide an explanation for the essentiality of BamD for the function of WT BamA, which also might interact with the substrate (70, 71). The exact role of the other lipoproteins remains to be elucidated and they might be required to facilitate and/or accelerate the folding of diverse substrates in the physiological environments (5, 53, 72, 73). The possibility to observe BAM in *E. coli* and in the native outer membranes (34, 74, 75) provides a great opportunity to elucidate the dynamic basis of BAM function (76) as well as its inhibition by novel compounds, antibodies, and nanobodies, etc. (77), in the native asymmetric bilayers.

Materials and methods

Plasmid construction and mutagenesis

The plasmid pJH114 (78) that encodes the BamABCDE full complex and pSK86 (79) encoding BamAB subcomplex was provided by Marc Baldus. The plasmid pJH114 was used to create the plasmid pJH114- Δ B encoding BamACDE by deleting the *bamB* gene using the Q5 site-directed mutagenesis kit (New England Biolabs). The *bamA* gene, which includes an N-terminal His₆ tag and a thrombin cleavage site following the signal sequence, was custom synthesized (GeneArt, Thermo Fisher Scientific) and inserted into the pCDFDuet-1 vector to produce the *bamA*/pCDFDuet-1 plasmid (34). The *bamB* from pSK86 was cloned into pETDuet-1 vector to create the *bamB*/pETDuet-1 plasmid. The native cysteines (C690 and C700) of *bamA* were substituted to a serine to create the Cys-less variant. Cysteines were further introduced in *bamA* at the desired positions using the Q5 site-directed mutagenesis kit.

Protein expression

The BamABCDE, BamACDE, and BamAB were expressed and purified using a protocol adapted from previous publications (63, 79). For BamABCDE and BamACDE expression, the plasmids pJH114 and pJH114- Δ B were transformed to BL21(DE3) competent cells.

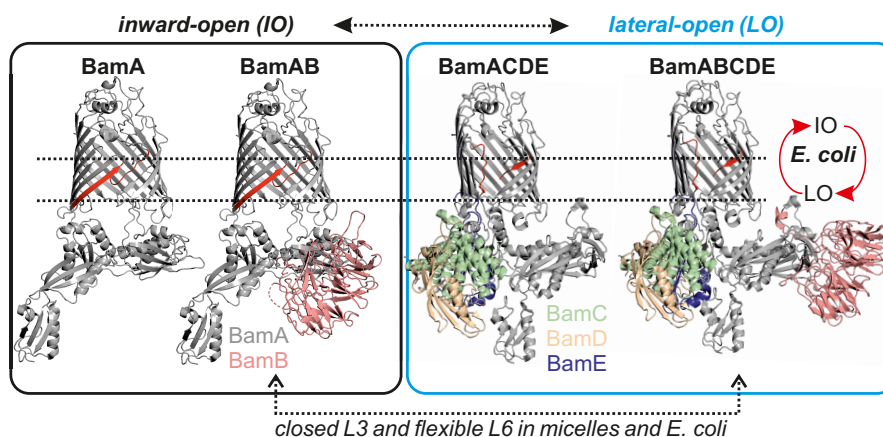


Fig. 7. Effect of lipoproteins on BamA and the conformational heterogeneity of BAM in *E. coli*. In detergent micelles, BamA and the BamAB subcomplex exist in the IO conformation. The BamACDE and BamABCDE complexes adopt the LO conformation and the BamCDE subcomplex regulates the transition of BamA between these two major conformations. In *E. coli*, the BamABCDE complex exhibits an enhanced conformational heterogeneity. The lateral gate shows a broad distribution spanning both IO and LO conformations. Overall, the extracellular loop 3 (L3) has a closed conformation and in the absence of the native disulfide bond, L6 displays large segmental flexibility for BamAB, BamACDE, and BamABCDE complexes in both micelles and *E. coli*. In the native membranes, BamCDE binding might enhance lateral opening of BamA and subsequent protein insertion.

Cells were grown in Lysogeny broth (LB) media containing 50 $\mu\text{g}/\text{mL}$ ampicillin at 37 °C until an OD_{600} of 0.6–0.8. The culture was then diluted 1:100 times to 2 \times Yeast Extract Tryptone medium (YT) media (16 g/L tryptone, 10 g/L yeast extract, and 5 g/L NaCl) and grown at 37 °C until an OD_{600} of \sim 0.7 is reached. Protein expression was induced with 0.4 mM isopropyl β -D-1-thiogalactopyranoside (IPTG) and grown further for 1.5 h. For BamAB expression, the plasmids *bamA/pCDFDuet-1* and *bamB/pETDuet-1* were cotransformed to BL21(DE3) competent cells. Expression was carried out in a similar manner in the presence of 50 $\mu\text{g}/\text{mL}$ streptomycin and 50 $\mu\text{g}/\text{mL}$ ampicillin.

Protein purification and spin labeling

Cell cultures obtained were spun down at 8,000 $\times g$ for 10 min and resuspended in 20 mL lysis buffer (20 mM Tris-HCl pH 8.0, 100 $\mu\text{g}/\text{mL}$ lysozyme, 1 mM phenylmethylsulfonyl fluoride [PMSF], and 1 $\mu\text{g}/\text{mL}$ DNaseI) per gram of cells. Cells were lysed using sonication and then pelleted down at 10,000 $\times g$ for 20 min. About 0.5% N-laurylsarcosine sodium salt was added to the supernatant to solubilize the inner membrane and stirred at room temperature for 10 min. The solution was then ultracentrifuged at 200,000 $\times g$ for 1.5 h. The resulting OM pellet was resuspended in the B20 buffer (20 mM Tris-HCl pH 8.0, 300 mM NaCl, 20 mM imidazole, 1% DDM, and 1 mM PMSF, 100 mL/g cells) for 1 h. The suspension was then ultracentrifuged at 200,000 $\times g$ for 30 min. The supernatant was incubated with 2 mL Ni-Sepharose High Performance slurry (GE Healthcare) for 1 h. The mixture was then loaded onto a PD-10 empty column (GE Healthcare) and washed with 2.5 column volumes B20 buffer containing 5 mM β -mercaptoethanol followed by 5–7 column volumes of B30 buffer (20 mM Tris-HCl pH 8.0, 150 mM NaCl, 30 mM imidazole, 0.1% DDM, and 5 mM β -mercaptoethanol). The protein was eluted using five-column volumes of B200 buffer (20 mM Tris-HCl pH 8.0, 150 mM NaCl, 200 mM imidazole, 0.1% DDM, and 5 mM β -mercaptoethanol). The eluted protein was buffer exchanged to 20 mM Tris-HCl pH 8.0, 150 mM NaCl, and 0.1% DDM using a PD-10 desalting column (GE Healthcare). The desalted protein was immediately mixed with a 40-fold excess of the spin label, 1-oxyl-2,2,5,5-tetramethyl-3-pyrroline-3-methyl methanethiosulfonate (MTSL, Toronto Research Chemicals) and kept stirring at room temperature for 30 min. The labeled protein was then concentrated in Vivaspin 6 concentrators (Molecular weight cut-off [MWCO] of 50,000 Da for BamAB and BamACDE, and MWCO 100,000 Da for ABCDE) and subsequently applied to a Superdex 200 Increase 10/300 GL column (GE Healthcare). The eluted protein fractions were further concentrated to 12–30 μM before sample preparation.

Protein expression and spin labeling in *E. coli*

For in situ measurements, the plasmid pJH114 encoding the genes for BamABCDE was transformed into *E. coli* BL21(DE3) cells. A pre-culture of 20 mL LB media containing 50 $\mu\text{g}/\text{mL}$ ampicillin was prepared and grown at 37 °C until an OD_{600} of 0.6. 1 mL of the pre-culture was inoculated to 100 mL of 2 \times YT media and grown further to an OD_{600} of \sim 0.7. Cells were then induced with 0.4 mM IPTG and grown for 1.5 h. The OD_{600} of the culture was measured. An appropriate amount of culture was taken out, spun down at 7,000 $\times g$ for 10 min, and resuspended in 40 mL cold 3-(N-morpholino)propanesulfonic acid (MOPS)-NaCl buffer (50 mM MOPS pH 7.5 and 60 mM NaCl) to a final OD_{600} of 0.5. Cells were labeled by incubating with 10 μM MTSL for 15 min at room temperature with mixing. The cell suspension was then pelleted down at 7,000 $\times g$ for 10 min. To remove the excess MTSL, cells were

washed by pelleting and resuspending in 1.5 mL buffer twice. For CW ESR measurement, the final cell pellet was suspended in \sim 40 μL buffer. For PELDOR measurements, the cells were made to a final volume of \sim 30 μL using buffer and 15% d_8 -glycerol. OMPs are naturally devoid of reactive cysteines, which enables selective labeling and distance measurements for a site-specifically engineered cysteine pair (55, 56). The background signals when present do not result in any specific distances due to their random distribution, albeit somewhat reducing the overall sensitivity (34, 37). In detergent micelles, the labeling efficiency is estimated from the spin and the protein concentrations, respectively (see Table S1). In *E. coli*, the effective labeling efficiency can be estimated from the modulation depth of the PELDOR data (37).

In vivo complementation assay

The effect of cysteine substitutions was checked using in vivo complementation in JCM166 (4) cells provided by Sebastian Hiller. The plasmid *bamA/pCDFDuet-1* containing the substitutions was transformed to JCM166 cells and plated on LB agar containing 50 $\mu\text{g}/\text{mL}$ spectinomycin and 0.05% arabinose. A single colony from the plate was inoculated to 5 mL LB media containing 50 $\mu\text{g}/\text{mL}$ spectinomycin and 0.05% arabinose and grown at 37 °C until the OD_{600} reached \sim 1.5. Cell culture was then washed twice to remove the arabinose by pelleting down at 4,000 $\times g$ for 10 min and resuspending in LB media. Cells were resuspended in LB to a final OD_{600} of 1.0 and serial dilutions of 10, 100, 1,000, 10,000, and 100,000 folds were prepared. Two microliters of each dilution were then spotted onto LB agar plates containing 50 $\mu\text{g}/\text{mL}$ spectinomycin with or without 0.05% arabinose (34, 80).

LILBID-MS

For mass spectrometric analysis by LILBID-MS (39), the samples were buffer exchanged into 20 mM Tris-HCl, 50 mM NaCl, 0.1% DDM, and pH 8.0. For each measurement, 4 μL of the 10 μM sample was directly loaded into a piezo-driven droplet generator (MD-K-130, Microdrop Technologies GmbH, Germany). Droplets of around 50 μm diameter are produced by this generator with a frequency of 10 Hz at 100 mbar. These droplets are transferred into vacuum and irradiated by an infrared laser pulse, leading to an explosive expansion of the droplet and a release of the solvated ions. The IR laser runs at a wavelength of 2.8 μm and was set to a maximum energy output of 23 mJ per pulse with a pulse length of 6 ns. The released ions were accelerated by a Wiley-McLaren type ion optic for analysis by a home build time-of-flight setup. The voltage in the ion source was set to -4.0 kV between the first (repeller) and the second lenses. The third plate was grounded. Between 5 and 20 μs (delayed extraction time) after the irradiation the repeller was pulsed to -6.6 kV for 370 μs . The reflectron was set to -7.2 kV. The detector is a Daly-type, optimized for high m/z . Processing of spectra was done by using Massign, a software based on Labview (38).

RT CW ESR spectroscopy

A Bruker EMXnano benchtop spectrometer operating at the X-band frequency was used to conduct continuous wave ESR measurements at room temperature. A 20–40 μL sample was used in a micropipette (BRAND, Germany, with a diameter of 0.68, 0.86, or 1.2 mm). The CW ESR spectra were acquired with 100 kHz modulation frequency, 0.6–2 mW microwave power, 0.15 mT modulation amplitude, and 18 mT sweep width. In situ samples were subjected to signal averaging over 40 scans, while protein samples were averaged over 50 to 150 scans.

Pulsed ESR spectroscopy and data analysis

Pulsed ESR experiments were performed on a Bruker Elexsys E580 Q-Band Pulsed ESR spectrometer with SpinJet AWG equipped with an arbitrary waveform generator (AWG), a 50-W solid-state amplifier, a continuous-flow helium cryostat, and a temperature control system (Oxford Instruments). A 15–20 μL sample containing 15% d_8 -glycerol was transferred into a 1.6-mm outer diameter quartz EPR tube (Suprasil, Wilmad-LabGlass) and snap-frozen in liquid nitrogen. Measurements were performed at 50 K using a dead-time free four-pulse sequence and a 16-step phase cycling ($x[x][x_p]x$) (81). A 38 ns Gaussian pulse set to the maximum of the echo-detected field-swept spectrum was used as the pump pulse. The 48 ns Gaussian observer pulses were set at 80 MHz lower than the pump pulse. The deuterium modulations were averaged by increasing the first interpulse delay by 16 ns for eight steps. The dipolar evolution time window was adjusted based on the observed phase memory time T_M , which was determined using 48 ns $\pi/2 - \tau - \pi$ Gaussian pulses and a two-step phase cycling, while τ was increased in 4 ns steps.

Data analysis was performed using the DeerAnalysis 2022, DeerNet, or the DeerLab program as specified (52, 59, 60). For DeerLab, the primary data were fitted with a nonparametric distribution and a homogenous background using Tikhonov regularization (TR), and the uncertainty was estimated using bootstrapping. Data analysis employing TR was performed as implemented in the MATLAB-based DeerAnalysis 2022 package. The background function arising from the intermolecular interactions was removed from the primary data $V(t)/V(0)$ to obtain the form factor $F(t)/F(0)$. The resulting form factor was fitted with a model free TR to obtain the distance distribution. Error estimation of the probability distribution was determined using the validation procedure wherein the background time window and/or the dimensionality of the spin distribution was gradually changed (see Table S2). Data analysis was also performed with a user-independent approach employing deep neural network (DeerNet Spinach SVN Rev 5662) as implemented in DeerAnalysis package. Distance distributions were simulated employing a rotamer library approach using the MATLAB-based MMM2021.1 software package (82). BAM structures in the IO (PDB 5D00), LO (PDB 5LJO), and substrate-bound (PDB 6V05 and 7TTC) conformations were used for the simulations.

Acknowledgments

A.G. and B.J. thank Marc Baldus for providing pJH114 and pSK86 plasmids and initial expression/purification protocols and Sebastian Hiller for providing *E. coli* JCM166 cells.

Supplementary Material

Supplementary material is available at PNAS Nexus online.

Funding

This work was financially supported by the Deutsche Forschungsgemeinschaft via the Emmy Noether program (JO 1428/1–1), SFB 1507—“Membrane-associated Protein Assemblies, Machineries, and Supercomplexes,” and a large equipment fund (438280639) to B.J. N.M. acknowledges support from Deutsche Forschungsgemeinschaft (426191805).

Author Contributions

A.G. performed all the biochemical and ESR spectroscopy experiments. T.R. and N.M. performed and analyzed the LILBID–MS experiments. A.G. and B.J. designed the experiments, analyzed the data, and wrote the paper with inputs from T.R. and N.M. B.J. conceived the idea, acquired funding, supervised, and administered the project.

Preprints

This manuscript was posted on a preprint: <https://doi.org/10.1101/2023.08.13.553113>.

Data Availability

The raw data generated from this study are available upon request to the corresponding author.

References

- Mulani MS, Kamble EE, Kumkar SN, Tawre MS, Pardesi KR. 2019. Emerging strategies to combat ESKAPE pathogens in the era of antimicrobial resistance: a review. *Front Microbiol.* 10:539.
- Fairman JW, Noinaj N, Buchanan SK. 2011. The structural biology of beta-barrel membrane proteins: a summary of recent reports. *Curr Opin Struct Biol.* 21:523–531.
- Walther DM, Rapaport D, Tommassen J. 2009. Biogenesis of beta-barrel membrane proteins in bacteria and eukaryotes: evolutionary conservation and divergence. *Cell Mol Life Sci.* 66:2789–2804.
- Wu T, et al. 2005. Identification of a multicomponent complex required for outer membrane biogenesis in *Escherichia coli*. *Cell.* 121:235–245.
- Doyle MT, Bernstein HD. 2022. Function of the Omp85 superfamily of outer membrane protein assembly factors and polypeptide transporters. *Ann Rev Microbiol.* 76:259–279.
- Lundquist K, Billings E, Bi M, Wellnitz J, Noinaj N. 2021. The assembly of beta-barrel membrane proteins by BAM and SAM. *Mol Microbiol.* 115:425–435.
- Webb CT, Heinz E, Lithgow T. 2012. Evolution of the beta-barrel assembly machinery. *Trends Microbiol.* 20:612–620.
- Konovalova A, Kahne DE, Silhavy TJ. 2017. Outer membrane biogenesis. *Ann Rev Microbiol.* 71:539–556.
- Ranava D, Caumont-Sarcos A, Albenne C, Ieva R. 2018. Bacterial machineries for the assembly of membrane-embedded beta-barrel proteins. *FEMS Microbiol Lett.* 365:fny087.
- Wu RR, et al. 2021. Plasticity within the barrel domain of BamA mediates a hybrid-barrel mechanism by BAM. *Nat Commun.* 12:7131.
- Noinaj N, et al. 2013. Structural insight into the biogenesis of beta-barrel membrane proteins. *Nature.* 501:385–390.
- Noinaj N, Fairman JW, Buchanan SK. 2011. The crystal structure of BamB suggests interactions with BamA and its role within the BAM complex. *J Mol Biol.* 407:248–260.
- Kim KH, Aulakh S, Paetzel M. 2011. Crystal structure of beta-barrel assembly machinery BamCD protein complex. *J Biol Chem.* 286:39116–39121.
- Knowles TJ, et al. 2011. Structure and function of BamE within the outer membrane and the beta-barrel assembly machine. *EMBO Rep.* 12:123–128.
- Ni D, et al. 2014. Structural and functional analysis of the beta-barrel domain of BamA from *Escherichia coli*. *FASEB J.* 28:2677–2685.

- 16 Albrecht R, et al. 2014. Structure of BamA, an essential factor in outer membrane protein biogenesis. *Acta Crystallogr D Biol Crystallogr*. 70:1779–1789.
- 17 Gruss F, et al. 2013. The structural basis of autotransporter translocation by TamA. *Nat Struct Mol Biol*. 20:1318–1320.
- 18 Bakelar J, Buchanan SK, Noinaj N. 2016. The structure of the beta-barrel assembly machinery complex. *Science*. 351:180–186.
- 19 Gu Y, et al. 2016. Structural basis of outer membrane protein insertion by the BAM complex. *Nature*. 531:64–69.
- 20 Iadanza MG, et al. 2016. Lateral opening in the intact β -barrel assembly machinery captured by cryo-EM. *Nat Commun*. 7:12865.
- 21 Schiffrin B, et al. 2022. Dynamic interplay between the periplasmic chaperone SurA and the BAM complex in outer membrane protein folding. *Commun Biol*. 5:560.
- 22 Sklar JG, Wu T, Kahne D, Silhavy TJ. 2007. Defining the roles of the periplasmic chaperones SurA, Skp, and DegP in *Escherichia coli*. *Gene Dev*. 21:2473–2484.
- 23 Tomasek D, et al. 2020. Structure of a nascent membrane protein as it folds on the BAM complex. *Nature*. 583:473–478.
- 24 Doyle MT, et al. 2022. Cryo-EM structures reveal multiple stages of bacterial outer membrane protein folding. *Cell*. 185:1143–1156.e13.
- 25 Shen C, et al. 2023. Structural basis of BAM-mediated outer membrane beta-barrel protein assembly. *Nature*. 617:185–193.
- 26 Imai Y, et al. 2019. A new antibiotic selectively kills Gram-negative pathogens. *Nature*. 576:459–464.
- 27 Kaur H, et al. 2021. The antibiotic darobactin mimics a beta-strand to inhibit outer membrane insertase. *Nature*. 593:125–129.
- 28 Luther A, et al. 2019. Chimeric peptidomimetic antibiotics against gram-negative bacteria. *Nature*. 576:452–458.
- 29 Hart EM, et al. 2019. A small-molecule inhibitor of BamA impervious to efflux and the outer membrane permeability barrier. *Proc Natl Acad Sci U S A*. 116:21748–21757.
- 30 Hagan CL, Wzorek JS, Kahne D. 2015. Inhibition of the beta-barrel assembly machine by a peptide that binds BamD. *Proc Natl Acad Sci U S A*. 112:2011–2016.
- 31 Iadanza MG, et al. 2016. Lateral opening in the intact beta-barrel assembly machinery captured by cryo-EM. *Nat Commun*. 7:12865.
- 32 Noinaj N, Kuszak AJ, Balusek C, Gumbart JC, Buchanan SK. 2014. Lateral opening and exit pore formation are required for BamA function. *Structure*. 22:1055–1062.
- 33 Lundquist K, Bakelar J, Noinaj N, Gumbart JC. 2018. C-terminal kink formation is required for lateral gating in BamA. *Proc Natl Acad Sci U S A*. 115:E7942–E7949.
- 34 Gopinath A, Joseph B. 2022. Conformational flexibility of the protein insertase BamA in the native asymmetric bilayer elucidated by ESR spectroscopy. *Angew Chem Int Ed Engl*. 61:e202113448.
- 35 Ketter S, Joseph B. 2023. Gd(3+)-trityl-nitroxide triple labeling and distance measurements in the heterooligomeric cobalamin transport complex in the native lipid bilayers. *J Am Chem Soc*. 145:960–966.
- 36 Ketter S, et al. 2022. In situ distance measurements in a membrane transporter using maleimide functionalized orthogonal spin labels and 5-pulse electron-electron double resonance spectroscopy. *J Magn Reson Open*. 10:100041.
- 37 Joseph B, et al. 2019. In situ observation of conformational dynamics and protein ligand-substrate interactions in outer-membrane proteins with DEER/PELDOR spectroscopy. *Nat Protoc*. 14:2344–2369.
- 38 Morgner N, Robinson CV. 2012. Massign: an assignment strategy for maximizing information from the mass spectra of heterogeneous protein assemblies. *Anal Chem*. 84:2939–2948.
- 39 Morgner N, Barth HD, Brutschy B. 2006. A new way to detect non-covalently bonded complexes of biomolecules from liquid microdroplets by laser mass spectrometry. *Aust J Chem*. 59:109–114.
- 40 Galazzo L, Bordignon E. 2023. Electron paramagnetic resonance spectroscopy in structural-dynamic studies of large protein complexes. *Prog Nucl Magn Reson Spectrosc*. 134–135:1–19.
- 41 Goldfarb D. 2022. Exploring protein conformations in vitro and in cell with EPR distance measurements. *Curr Opin Struct Biol*. 75:102398.
- 42 Del Alamo D, Sala D, McHaourab HS, Meiler J. 2022. Sampling alternative conformational states of transporters and receptors with AlphaFold2. *Elife*. 11:e75751.
- 43 Pierro A, Drescher M. 2023. Dance with spins: site-directed spin labeling coupled to electron paramagnetic resonance spectroscopy directly inside cells. *Chem Comm*. 59:1274–1284.
- 44 Bonucci A, Ouari O, Guigliarelli B, Belle V, Mileo E. 2020. In-Cell EPR: progress towards structural studies inside cells. *ChemBioChem*. 21:451–460.
- 45 Schiemann O, et al. 2021. Benchmark test and guidelines for DEER/PELDOR experiments on nitroxide-labeled biomolecules. *J Am Chem Soc*. 143:17875–17890.
- 46 Pannier M, Veit S, Godt A, Jeschke G, Spiess HW. 2000. Dead-time free measurement of dipole-dipole interactions between electron spins. *J Magn Reson*. 142:331–340.
- 47 Hubbell WL, McHaourab HS, Altenbach C, Lietzow MA. 1996. Watching proteins move using site-directed spin labeling. *Structure*. 4:779–783.
- 48 Stoll S, Schweiger A. 2006. EasySpin, a comprehensive software package for spectral simulation and analysis in EPR. *J Magn Reson*. 178:42–55.
- 49 Pinto C, et al. 2018. Formation of the beta-barrel assembly machinery complex in lipid bilayers as seen by solid-state NMR. *Nat Commun*. 9:4135.
- 50 Leonard-Rivera M, Misra R. 2012. Conserved residues of the putative L6 loop of *Escherichia coli* BamA play a critical role in the assembly of beta-barrel outer membrane proteins, including that of BamA itself. *J Bacteriol*. 194:4662–4668.
- 51 Morgado L, Zeth K, Burmann BM, Maier T, Hiller S. 2015. Characterization of the insertase BamA in three different membrane mimetics by solution NMR spectroscopy. *J Biomol NMR*. 61:333–345.
- 52 Fabregas Ibanez L, Jeschke G, Stoll S. 2020. DeerLab: a comprehensive software package for analyzing dipolar electron paramagnetic resonance spectroscopy data. *Magn Reson (Gott)*. 1:209–224.
- 53 White P, et al. 2021. The role of membrane destabilisation and protein dynamics in BAM catalysed OMP folding. *Nat Commun*. 12:4174.
- 54 Hartmann JB, Zahn M, Burmann IM, Bibow S, Hiller S. 2018. Sequence-specific solution NMR assignments of the beta-barrel insertase BamA to monitor its conformational ensemble at the atomic level. *J Am Chem Soc*. 140:11252–11260.
- 55 Joseph B, Sikora A, Cafiso DS. 2016. Ligand induced conformational changes of a membrane transporter in *E. coli* cells observed with DEER/PELDOR. *J Am Chem Soc*. 138:1844–1847.
- 56 Joseph B, et al. 2015. Distance measurement on an endogenous membrane transporter in *E. coli* cells and native membranes using EPR spectroscopy. *Angew Chem Int Ed Engl*. 54:6196–6199.
- 57 Ritzmann N, Manioglu S, Hiller S, Muller DJ. 2022. Monitoring the antibiotic darobactin modulating the beta-barrel assembly factor BamA. *Structure*. 30:350–359.e353.

- 58 Narasimhan S, et al. 2021. Characterizing proteins in a native bacterial environment using solid-state NMR spectroscopy. *Nat Protoc.* 16:893–918.
- 59 Worswick SG, Spencer JA, Jeschke G, Kuprov I. 2018. Deep neural network processing of DEER data. *Sci Adv.* 4:eaat5218.
- 60 Jeschke G, et al. 2006. DeerAnalysis2006—a comprehensive software package for analyzing pulsed ELDOR data. *Appl Magn Reson.* 30:473–498.
- 61 Li GW, Burkhardt D, Gross C, Weissman JS. 2014. Quantifying absolute protein synthesis rates reveals principles underlying allocation of cellular resources. *Cell.* 157:624–635.
- 62 Ojkic N, Serbanescu D, Banerjee S. 2019. Surface-to-volume scaling and aspect ratio preservation in rod-shaped bacteria. *Elife.* 8:e47033.
- 63 Han L, et al. 2016. Structure of the BAM complex and its implications for biogenesis of outer-membrane proteins. *Nat Struct Mol Biol.* 23:192–196.
- 64 Rodriguez-Alonso R, et al. 2020. Structural insight into the formation of lipoprotein-beta-barrel complexes. *Nat Chem Biol.* 16:1019–1025.
- 65 Liu J, Gumbart JC. 2020. Membrane thinning and lateral gating are consistent features of BamA across multiple species. *PLoS Comput Biol.* 16:e1008355.
- 66 Schiffrin B, et al. 2017. Effects of periplasmic chaperones and membrane thickness on BamA-catalyzed outer-membrane protein folding. *J Mol Biol.* 429:3776–3792.
- 67 Gessmann D, et al. 2014. Outer membrane beta-barrel protein folding is physically controlled by periplasmic lipid head groups and BamA. *Proc Natl Acad Sci U S A.* 111:5878–5883.
- 68 Patel GJ, Kleinschmidt JH. 2013. The lipid bilayer-inserted membrane protein BamA of *Escherichia coli* facilitates insertion and folding of outer membrane protein A from its complex with Skp. *Biochemistry.* 52:3974–3986.
- 69 Danoff EJ, Fleming KG. 2015. Membrane defects accelerate outer membrane beta-barrel protein folding. *Biochemistry.* 54:97–99.
- 70 Lee J, et al. 2018. Substrate binding to BamD triggers a conformational change in BamA to control membrane insertion. *Proc Natl Acad Sci U S A.* 115:2359–2364.
- 71 Hart EM, Gupta M, Wuhr M, Silhavy TJ. 2020. The gain-of-function allele bamA(E470K) bypasses the essential requirement for BamD in beta-barrel outer membrane protein assembly. *Proc Natl Acad Sci U S A.* 117:18737–18743.
- 72 Plummer AM, Fleming KG. 2015. BamA alone accelerates outer membrane protein folding in vitro through a catalytic mechanism. *Biochemistry.* 54:6009–6011.
- 73 Misra R, Stikeleather R, Gabriele R. 2015. In vivo roles of BamA, BamB and BamD in the biogenesis of BamA, a core protein of the beta-barrel assembly machine of *Escherichia coli*. *J Mol Biol.* 427:1061–1074.
- 74 Ketter S, et al. 2021. In situ labeling and distance measurements of membrane proteins in *E. coli* using Finland and OX063 trityl labels. *Chemistry.* 27:2299–2304.
- 75 Haysom SF, et al. 2023. Darobactin B stabilises a lateral-closed conformation of the BAM Complex in *E. coli* cells. *Angew Chem Int Ed Engl.* 62:e202218783.
- 76 Wu R, Stephenson R, Gichaba A, Noinaj N. 2020. The big BAM theory: an open and closed case? *Biochim Biophys Acta Biomembr.* 1862:183062.
- 77 Overly Cottom C, Stephenson R, Wilson L, Noinaj N. 2023. Targeting BAM for novel therapeutics against pathogenic gram-negative bacteria. *Antibiotics.* 12:679.
- 78 Roman-Hernandez G, Peterson JH, Bernstein HD. 2014. Reconstitution of bacterial autotransporter assembly using purified components. *Elife.* 3:e04234.
- 79 Hagan CL, Kim S, Kahne D. 2010. Reconstitution of outer membrane protein assembly from purified components. *Science.* 328:890–892.
- 80 Xiao L, et al. 2021. Structures of the beta-barrel assembly machine recognizing outer membrane protein substrates. *FASEB J.* 35:e21207.
- 81 Tait CE, Stoll S. 2016. Coherent pump pulses in double electron electron resonance spectroscopy. *Phys Chem Chem Phys.* 18:18470–18485.
- 82 Jeschke G. 2021. MMM: integrative ensemble modeling and ensemble analysis. *Protein Sci.* 30:125–135.